

## SUPPLEMENTARY INFORMATION

# Boosting the capacity of Mg-stabilized $\text{Na}_{0.66}\text{Ni}_{0.27}\text{Mg}_{0.06}\text{Mn}_{0.66}\text{O}_2$ cathodes via particle size control in an emulsion-based synthesis route

Saúl Rubio,<sup>a</sup> Eva M. Pérez-Soriano,<sup>b</sup> Cristina Arévalo,<sup>b</sup> Xiaoqiong Du,<sup>c</sup> Xuyun Guo,<sup>c</sup> Francisco J. García-García,<sup>a</sup> Isabel Montealegre-Meléndez,<sup>a</sup> Ana M. Beltrán,<sup>a</sup> Valeria Nicolosi<sup>c</sup> and Juan G. Lozano\*<sup>a</sup>

<sup>a</sup> Departamento de Ingeniería y Ciencia de los Materiales y del Transporte, Escuela Politécnica Superior/CATEPS, Universidad de Sevilla, Sevilla (Spain)

<sup>b</sup> Departamento de Ingeniería y Ciencia de los Materiales y del Transporte, Escuela Técnica Superior de Ingeniería, Universidad de Sevilla, Sevilla (Spain)

<sup>c</sup> School of Chemistry, Centre for Research on Adaptive Nanostructures and Nanodevices (CRANN) and Advanced Materials Bio-Engineering Research Centre (AMBER), Trinity College Dublin, Dublin (Ireland)

### 1. Rietveld analysis:

**Table S1.** Rietveld refinement parameters of the P2 and O3 phases exhibited for all samples.

Phase	Parameters	Sample			
		ST	HV	HW	HO
<b>P2</b>	a[Å]	2.87869(11)	2.88772(13)	2.8785(2)	2.88573(11)
	c[Å]	11.2348(10)	11.1781(13)	11.2205(18)	11.1965(10)
	R-Bragg	2.445	1.672	1.133	1.848
<i>Phase [%]</i>		86.6(6)	83.2(5)	73.8(9)	76.9(5)
<b>O3</b>	a[Å]	2.9070(17)	2.8827(9)	2.8959(16)	2.8809(6)
	c[Å]	16.954(7)	16.917(4)	16.848(9)	16.937(3)
	R-Bragg	3.016	2.811	1.289	2.53
<i>Phase [%]</i>		13.4(6)	16.8(5)	26.2(9)	23.1(5)
	$R_{wp}$	3.37	3.45	3.89	3.32
	$R_p$	2.49	2.60	2.79	2.55
	GOF( $\chi^2$ )	1.37	1.31	1.48	1.30

## 2. Compositional analysis:

To verify the chemical composition of the particles synthesised via the organic route, XRF measurements were performed. Table S2 shows the stoichiometric values obtained for the ST, HV, HW, and HO samples, with the oxygen content fixed at 2. The measured values agree well with the expected compositions, considering the instrumental error (5% for Na, Mn, and Ni, and 10% for Mg). To assess the elemental distribution, EDX mapping in STEM mode was carried out (Figure S1), confirming their homogeneous distribution within the particles.

**Table S2.** Stoichiometric values by XRF of the different samples.

Sample	Na	Mn	Ni	Mg
ST	0.659	0.671	0.284	0.045
HV	0.686	0.657	0.305	0.038
HW	0.663	0.669	0.278	0.054
HO	0.670	0.665	0.295	0.040

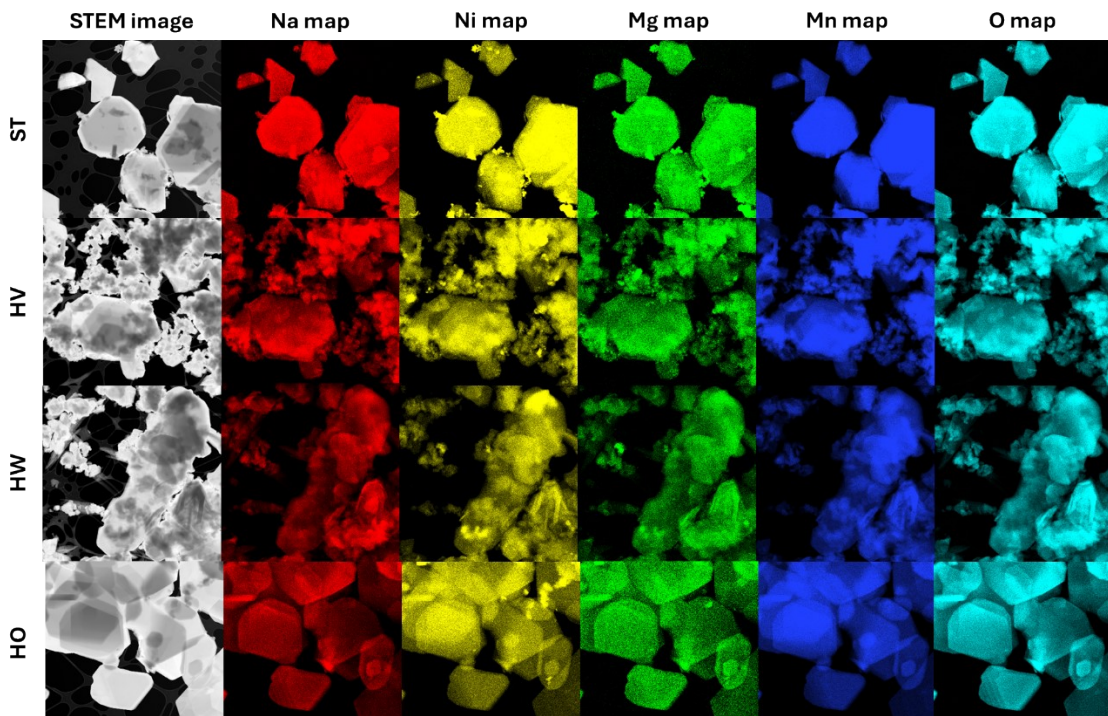


Figure S1: EDX compositional maps acquired in STEM mode, displaying the Na, Ni, Mg, Mn and O distribution within the ST, HV, HW and HO samples

### 3. Statistical analysis:

For the statistical analysis, the longest axis of 1000 particles was measured in each of the four samples using SEM micrographs taken from different regions. The measurements were performed using *ImageJ* software. The results are summarized in Figure S2.

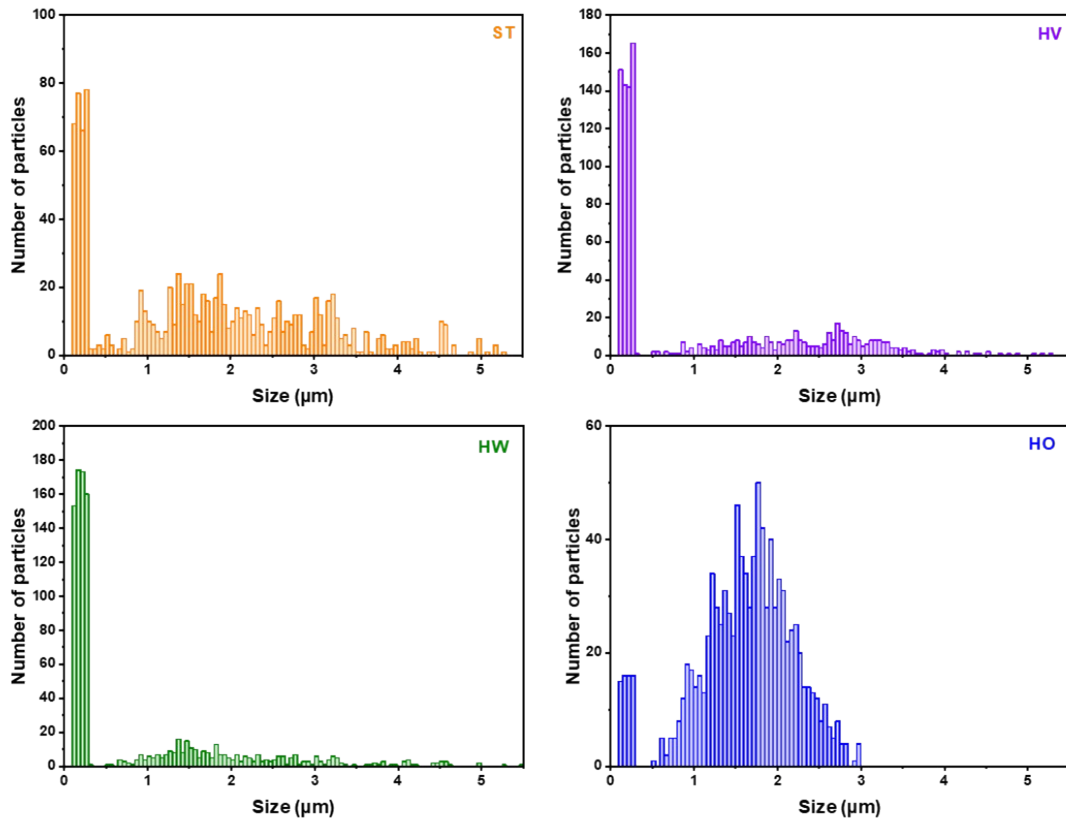


Figure S2: Histograms displaying the particle size distribution for the ST, HV, HW and HO samples.

#### 4. Characterisation of a $\text{Na}_{0.66}\text{Ni}_{0.27}\text{Mg}_{0.06}\text{Mn}_{0.66}\text{O}_2$ sample synthesised by conventional dry milling:

For comparison, a sample of  $\text{Na}_{0.66}\text{Ni}_{0.27}\text{Mg}_{0.06}\text{Mn}_{0.66}\text{O}_2$  was fabricated using a dry-milling route. For that, stoichiometric amounts of metal oxides were mixed in a milling jar and ball-milled in a *Retsch PM100* planetary ball mill for 90 minutes at 450 rpm, using a powder-to-balls ratio of 1:10 (in mass). The resulting mixture was then heated at  $900^\circ\text{C}$  for 10 hours. Cell-assembly and electrochemical characterisation was performed following the same procedure described in the experimental section of the main manuscript. The results are summarised in Figure S3. XRD measurements (Figure S3a) indicate that the synthesised particles consist predominantly of the P2 phase, with minor traces of the O3 phase, something that was confirmed via high resolution STEM (Figure S3c). SEM micrographs (Figure S3b) reveal that the particles exhibit a truncated hexagonal pyramidal shape. Analysis of the particle size distribution (inset in Figure S3b) shows that it follows a Gaussian distribution, with an average particle length (longest axis) of  $3.0 \mu\text{m}$  and a standard deviation of  $1.1 \mu\text{m}$ .

It can be seen from the electrochemical characterisation (Figure S3 d)-g), that the initial charge and discharge capacities of this sample are 148 and  $104 \text{ mA h g}^{-1}$  respectively. The charge and discharge after 100 cycles are 79 and  $77 \text{ mA h g}^{-1}$ .

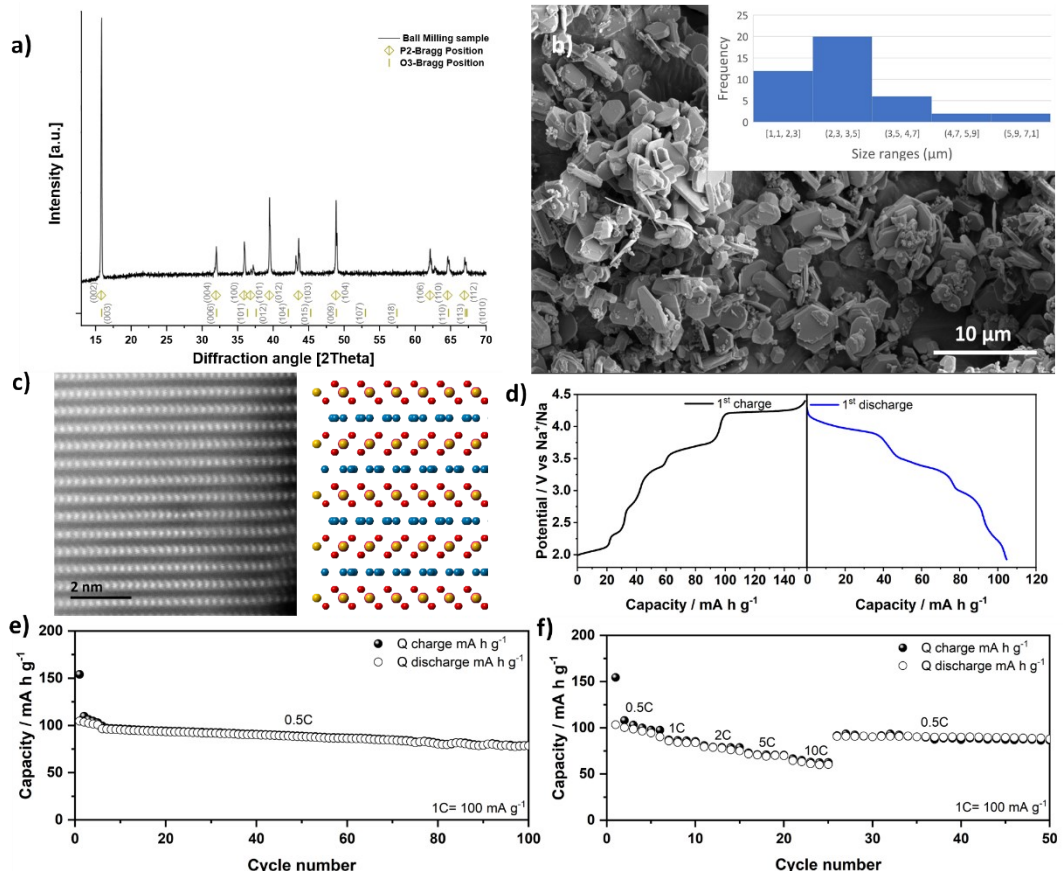


Figure S3: a) XRD spectrum from the  $\text{Na}_{0.66}\text{Ni}_{0.27}\text{Mg}_{0.06}\text{Mn}_{0.66}\text{O}_2$  fabricated using a dry-milling route. b) SEM micrograph of the synthesised particles and histogram of the particle size distribution (inset). c) High resolution STEM micrograph of a particle confirming the P2 structure. d) Galvanostatic first charge/discharge curve, e) retention capacity profiles of the during the first 100 cycles, and f) rate performance at room temperature.

**5. Supplementary Figures:**

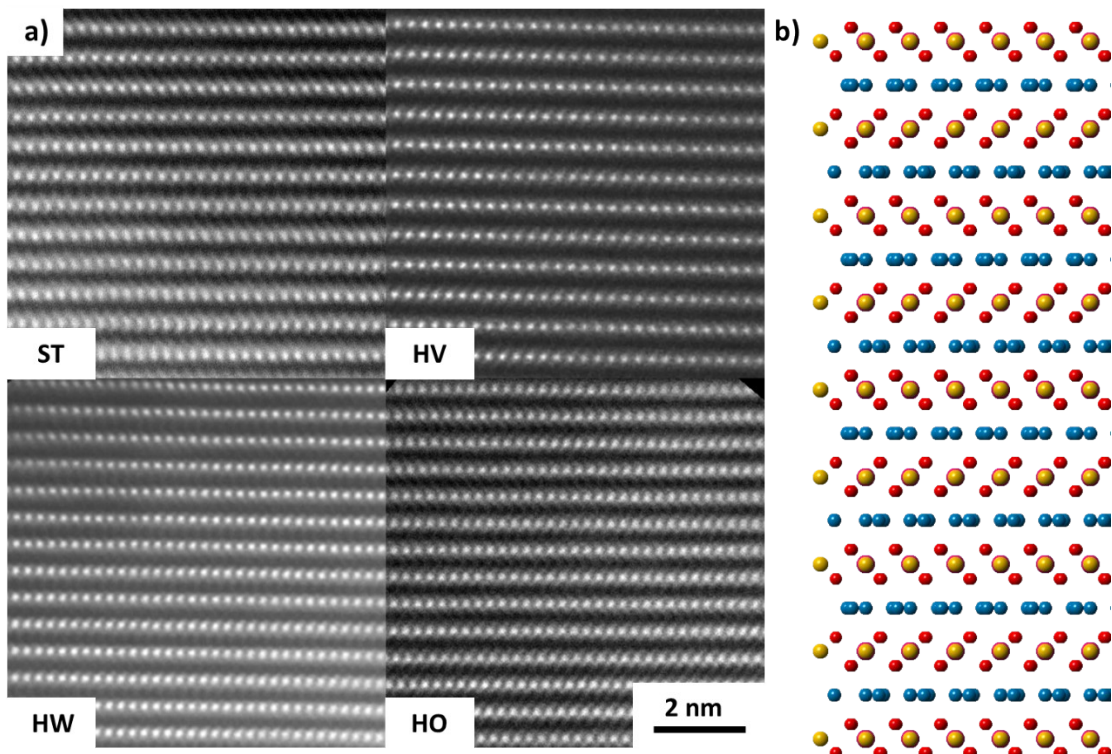


Figure S4: a) High resolution STEM micrographs of the ST, HV, HW and HO samples; b) atomic model of the P2 structure (transition metals in yellow, oxygen in red, sodium in blue).

## 6. Comparison with results reported in the literature:

**Table S3.** Review of results previously reported in the literature for Mg-doped Na-TMOs.

Reference	Compounds	Synthesis method	Current density [1C=100 mA g <sup>-1</sup> ]	1 <sup>st</sup> discharge capacity [mAh g <sup>-1</sup> ]	Long term discharge capacity [mAh g <sup>-1</sup> ]	Coulombic efficiency last cycle (%)
<i>Our work</i>	P2-Na <sub>0.67</sub> Ni <sub>0.27</sub> Mg <sub>0.06</sub> Mn <sub>0.66</sub> O <sub>2</sub>	Emulsion	0.5C	253	172 (100 cycles)	99
[1]	O3-Na <sub>0.9</sub> Ni <sub>0.23</sub> Mg <sub>0.12</sub> Mn <sub>0.6</sub> O <sub>2</sub>	Sol-gel	0.1C	179	145 (100 cycles)	90
[2]	P2-Na <sub>0.67</sub> Ni <sub>0.23</sub> Mg <sub>0.1</sub> Mn <sub>0.67</sub> O <sub>2</sub>	Sol-gel	0.5C	108	87 (100 cycles)	-
[3]	P2-Na <sub>0.67</sub> Ni <sub>0.25</sub> Mg <sub>0.1</sub> Mn <sub>0.65</sub> O <sub>2</sub>	Sol-gel	0.1C	140	122 (100 cycles)	98
[4]	P2-Na <sub>0.5</sub> Ni <sub>0.22</sub> Mg <sub>0.1</sub> Mn <sub>0.7</sub> O <sub>2</sub>	Sol-gel	0.1C	143	109 (50 cycles)	98
[5]	P2-Na <sub>0.67</sub> Ni <sub>0.28</sub> Mg <sub>0.05</sub> Mn <sub>0.67</sub> O <sub>2</sub>	Sol-gel	0.1C	123	105 (50 cycles)	98
[6]	P2/O3-Na <sub>0.8</sub> K <sub>0.05</sub> Ca <sub>0.05</sub> Ni <sub>0.2</sub> Fe <sub>0.2</sub> Mg <sub>0.05</sub> Mn <sub>0.55</sub> O <sub>2</sub>	Sol-gel	0.1C	143	117 (250 cycles)	99.8
[7]	P2-Na <sub>0.66</sub> Ni <sub>0.3</sub> Mg <sub>0.01</sub> Cr <sub>0.02</sub> Mn <sub>0.67</sub> O <sub>2</sub>	Wet ball-milling	0.1C	135	116 (50 cycles)	-
[8]	P2-Na <sub>0.67</sub> Ni <sub>0.225</sub> Mg <sub>0.075</sub> Mn <sub>0.67</sub> O <sub>2</sub>	Solid-state reaction	1C	167	86 (100 cycles)	-
[9]	P2-Na <sub>0.75</sub> Ni <sub>0.23</sub> Mg <sub>0.1</sub> Mn <sub>0.67</sub> O <sub>1.95</sub> F <sub>0.05</sub>	Sol-gel	1C	115	115 (100 cycles)	99.9
[10]	P2-Na <sub>0.62</sub> Ni <sub>0.15</sub> Mg <sub>0.1</sub> Mn <sub>0.75</sub> O <sub>2</sub>	Solid-state reaction	1C	159	146 (100 cycles)	99 <sup>11</sup>
[11]	P2/O3-Na <sub>0.67</sub> Cu <sub>0.2</sub> Mg <sub>0.1</sub> Fe <sub>0.2</sub> Mn <sub>0.5</sub> O <sub>2</sub>	Sol-gel	0.1C	212	187 (80 cycles)	99
[12]	P2/O3-Na <sub>0.9</sub> Fe <sub>0.24</sub> Mg <sub>0.25</sub> Mn <sub>0.35</sub> O <sub>2</sub>	Sol-gel	0.1C	150	95	-

- 1 K. Mathiyalagan, K. Karuppiah, A. Ponnaiah, S. Rengapillai and S. Marimuthu, *Int J Energy Res*, 2022, **46**, 10656–10667.
- 2 H. Hou, B. Gan, Y. Gong, N. Chen and C. Sun, *Inorg Chem*, 2016, **55**, 9033–9037.
- 3 K. Hemalatha, M. Jayakumar, P. Bera and A. S. Prakash, *J Mater Chem A Mater*, 2015, **3**, 20908–20912.
- 4 J. Zhang, H. Yuan, Z. Yang, Y. Huang, S. Kan, Y. Wu, P. He and H. Liu, *Ind Eng Chem Res*, 2019, **58**, 22804–22810.
- 5 P. Wang, Y. You, Y. Yin, Y. Wang, L. Wan, L. Gu and Y. Guo, *Angewandte Chemie*, 2016, **128**, 7571–7575.
- 6 Q. Meng, Q. Liu, K. Wang, X. Xu, W. Li and T. Hu, *J Colloid Interface Sci*, DOI:10.1016/j.jcis.2025.137437.
- 7 X. Xu, S. Hu, Q. Pan, Y. Huang, J. Zhang, Y. Chen, H. Wang, F. Zheng and Q. Li, *Small*, DOI:10.1002/smll.202307377.
- 8 Y. Duan, Z. Ma, L. Li, G. Su, S. Bao and J. Lu, *J Electrochem Soc*, 2024, **171**, 030502.
- 9 X. Wang, Z. Yang, D. Chen, B. Lu, Q. Zhang, Y. Hou, Z. Wu, Z. Ye, T. Li and J. Lu, *Adv Funct Mater*, DOI:10.1002/adfm.202418322.
- 10 P. Thanwisai, P. Vanaphuti, Z. Yao, J. Hou, Z. Meng, X. Ma, H. Guo, G. Gao, Z. Yang and Y. Wang, *Small*, DOI:10.1002/smll.202306465.
- 11 Y. Zhang, J. Chen, R. Wang, L. Wu, W. Song, S. Cao, Y. Shen, X. Zhang and X. Wang, *ACS Appl Mater Interfaces*, 2024, **16**, 11349–11360.
- 12 R. Klee, S. Rubio, P. Lavela and J. L. Tirado, *J Alloys Compd*, 2025, **1020**, 179385.